

## Helical Superstructures

## Chiral Perylene Diimides: Building Blocks for Ionic Self-Assembly

Geraldine Echue,<sup>[a]</sup> Guy C. Lloyd-Jones,<sup>[b]</sup> and Charl F. J. Faul\*<sup>[a]</sup>

**Abstract:** A chiral perylene diimide building block has been prepared based on an amine derivative of the amino acid L-phenylalanine. Detailed studies were carried out into the self-assembly behaviour of the material in solution and the solid state using UV/Vis, circular dichroism (CD) and fluorescence spectroscopy. For the charged building block BTPPP, the molecular chirality of the side chains is translated into the chiral supramolecular structure in the form of right-handed helical aggregates in aqueous solution. Temperature-dependent UV/Vis studies of BTPPP in aqueous solution showed that the self-assembly behaviour of this dye can be well described by an isodesmic model in which aggregation occurs to generate short stacks in a reversible manner. Wide-

angle X-ray diffraction studies (WXR) revealed that this material self-organises into aggregates with  $\pi$ - $\pi$  stacking distances typical for  $\pi$ -conjugated materials. TEM investigations revealed the formation of self-assembled structures of low order and with no expression of chirality evident. Differential scanning calorimetry (DSC) and polarised optical microscopy (POM) were used to investigate the mesophase properties. Optical textures representative of columnar liquid-crystalline phases were observed for solvent-annealed samples of BTPPP. The high solubility, tunable self-assembly and chiral ordering of these materials demonstrate their potential as new molecular building blocks for use in the construction of chiro-optical structures and devices.

## Introduction

The identification and preparation of suitable molecular building blocks (or tectons) for self-assembly enables the design and synthesis of new materials with tailored structure and function through rational choice of precursors.<sup>[1]</sup> Perylene diimides (PDIs), with their very well characterised self-assembly properties, are important building blocks in the realm of functional materials.<sup>[2,3]</sup> This class of functional materials have received much attention in recent years owing to their potential application as n-type semiconductors in optoelectronic devices such as solar cells,<sup>[4]</sup> field-effect transistors<sup>[5]</sup> and light-emitting diodes.<sup>[6]</sup> However, the behaviour of charged PDIs, particularly anisotropic core-unsubstituted PDIs that exhibit water solubility, is much less characterised.<sup>[7]</sup>

Chiral supramolecular assemblies have previously been produced using non-covalent interactions of chiral components such as nucleic acids<sup>[8]</sup> and ATP.<sup>[9]</sup> Chirality can alternatively be directly incorporated into PDI materials by substitution with

chiral side chains such as aliphatic amines,<sup>[10]</sup> amino acids,<sup>[11]</sup> and amino acid derivatives.<sup>[11d,12]</sup> The presence of chiral groups in perylene diimide materials often exerts steric demands on the possible arrangement of these planar  $\pi$ -conjugated units. Steric requirements, in combination with the favourable interactions between the central  $\pi$ -surfaces, typically result in the translation of chirality into helical supramolecular structures.<sup>[11b,13]</sup> Chiral assemblies have also been reported for PDIs and other discotic systems in which chiral amplification proceeds in a co-operative fashion by a 'sergeant and soldiers' or 'majority rules' effect.<sup>[14]</sup> The non-covalent nature of the intermolecular forces within the self-assembled aggregates enables properties of the assemblies to be modified by external factors such as solvent, temperature and concentration.<sup>[15]</sup>

Dehm et al. reported temperature-dependent changes in helicity for a chiral PDI derivative. By increasing the temperature, a characteristic switching from right-handed helical aggregates to left-handed helical dimers could be induced.<sup>[16]</sup> Hu et al. also showed that careful choice of solvent mixtures yielded either left- or right-handed helical nanostructures for sugar-derivatised PDIs, depending on the solvent ratio utilised.<sup>[17]</sup> The asymmetric properties of chiral PDI materials can lead to binding specificity for other anisotropic molecules such as lectin proteins, and is therefore especially relevant for applications requiring biocompatibility.<sup>[18]</sup> Chiral ordering also impacts on the electronic properties of PDI materials. Enhanced charge carrier mobility has previously been reported in discotic materials owing to the higher-order helical organisation of the molecular units.<sup>[16,19]</sup> Hu et al. showed, in a more recent study, that organic semiconductor materials based on chiral PDIs exhibited increased sensitivity relative to their achiral counterparts in

[a] Dr. G. Echue, Dr. C. F. J. Faul  
School of Chemistry, University of Bristol  
Bristol BS8 1TS (UK)  
E-mail: charl.faul@bristol.ac.uk

[b] Prof. G. C. Lloyd-Jones  
School of Chemistry, University of Edinburgh  
Edinburgh EH9 3JJ (UK)

Supporting information for this article is available on the WWW under <http://dx.doi.org/10.1002/chem.201406094>.

© 2015 The Authors. Published by Wiley-VCH Verlag GmbH & Co. KGaA. This is an open access article under the terms of the Creative Commons Attribution License, which permits use, distribution and reproduction in any medium, provided the original work is properly cited.

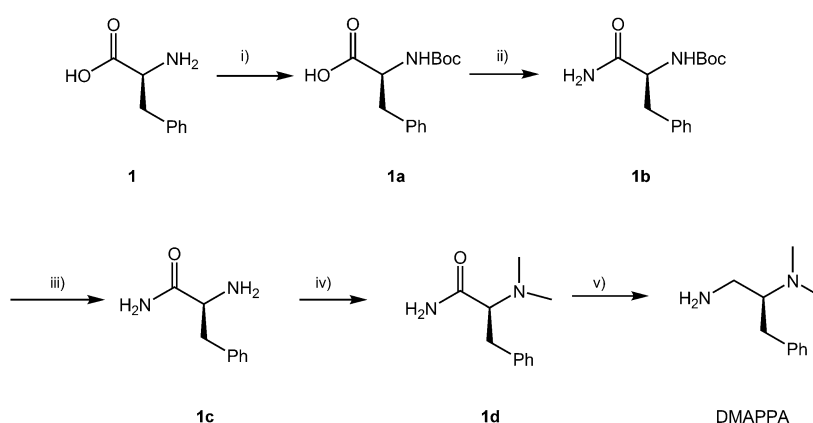
vapour-sensing devices.<sup>[17]</sup> All of these studies show inclusion of chirality in perylene diimide materials provide opportunities to tune structure, function and application.

Herein we describe the design and synthesis of a chiral PDI for use as a tecton in the production of supramolecular materials from ionic self-assembly (ISA).<sup>[20]</sup> ISA has been reported as a strategy for the production of liquid-crystalline materials based on complexation of a variety of oligo-,<sup>[21]</sup> polyelectrolytes<sup>[22]</sup> and charged PDIs<sup>[23]</sup> with oppositely charged surfactants. We demonstrated the induction of supramolecular chirality in the absence of chiral precursors in the case of metal-containing polyferrocenylsilane (PFS) polyelectrolyte complexes.<sup>[22]</sup> Previous chiral perylene diimide complexes prepared by ISA incorporated the chirality indirectly by means of a chiral surfactant. Franke et al obtained chiral, left-handed helical supramolecular architectures for ISA complexes based on lysine-derived surfactants.<sup>[24]</sup> In

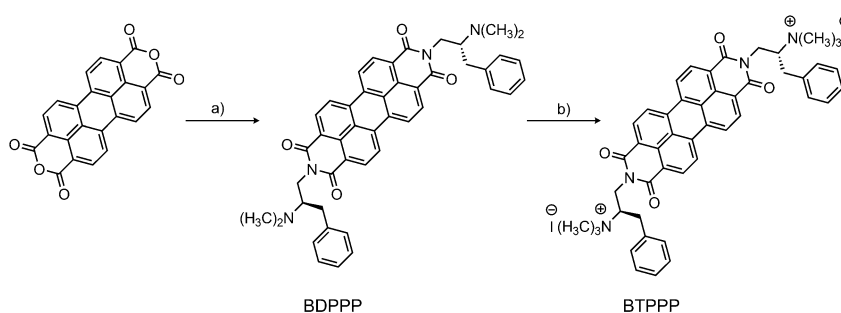
a separate study, solvent annealing of a chiral PDI-phosphate ISA complex synthesised by Huang et al, gave fan-shaped textures indicative of a columnar mesophase.<sup>[25]</sup> In contrast to previous ISA tectons, here for the first time, we investigate the effect of incorporating the chiral moiety directly into the PDI tecton. UV/Vis absorption, circular dichroism studies and microscopy were used to characterise the aggregation behaviour and mesophase properties of the chiral PDI in solution and the solid state. In this way, the effect of bringing the chiral centre closer to the perylene core can be explored for the production of self-assembled functional materials.

## Results and Discussion

An analogue of phenylalanine was synthesised in a six-step reaction procedure to give the chiral amine 2-*N,N*-dimethylamino-3-phenylpropanamine (DMAPPA) in good yield (Scheme 1, see the Supporting Information for detailed synthetic procedures). The synthesis of the target tecton *N,N*'-bis[2-(trimethylammonium)-3-(phenyl)propyl] perylene diimide (BTPPP) was accomplished by the reaction of the parent perylene dianhydride with an excess of the DMAPPA to give *N,N*'-bis[2-(dimethylamino)-3-(phenyl)propyl] perylene diimide (BDPPP). Methylation of the tertiary amine groups of BDPPP with methyl



**Scheme 1.** Synthesis of (*S*)-2-*N,N'*-dimethylamino-3-phenylpropanamine (DMAPPA): i) (Boc)<sub>2</sub>O, *t*BuOH, NaOH; 12 h; ii) DCC, HOBT, TEA, NH<sub>3</sub>, 0 °C, RT; 12 h; iii) acetyl chloride, MeOH; 0 °C 1 h; iv) H<sub>2</sub>, Pd/C (5%), CH<sub>2</sub>O 60–40 °C; 4 h; v) LiAlH<sub>4</sub>, dry THF; 23 h. DCC = *N,N'*-dicyclohexylcarbodiimide; HOBT = 1-hydroxybenzotriazole; TEA = triethylamine.



**Scheme 2.** Synthesis of perylene diimides BDPPP and BTPPP: a) 1-Butanol, DMAPPA, 90 °C, 24 h; b) Methyl iodide, DMF, 72 h.

iodide produced the charged tecton BTPPP (with an iodide counterion) in good yield (Scheme 2, see the Supporting Information for detailed synthetic procedures).

Coupling of the diastereotopic methylene protons of the bulky side chains is clearly observed in the NMR spectra of BDPPP (see the Supporting Information, Figure S7). The appearance of the coupling is most likely due to the reduction in the rotational freedom of these chains as a result of steric hindrance around the phenyl groups once the side chains are covalently bonded in close proximity to the perylene central unit. The NMR spectrum of BDPPP in chloroform exhibits highly resolved peaks corresponding to the aromatic protons of the central perylene unit indicative of reduced aggregation in this solvent. To further investigate the aggregation properties of both BDPPP and BTPPP, solution-state UV/Vis and CD studies were performed in various solvents.

### Photophysical studies of aggregation

BDPPP and BTPPP possess significantly different solubility properties due to the absence of charged groups for BDPPP. BDPPP is soluble in a wide range of common organic and mid-polarity solvents including chloroform and butanol, whereas BTPPP is insoluble in the same systems. The intensity and pat-

tern of absorption of PDIs have been widely used to characterise their behaviour in solution.<sup>[26]</sup> Aggregation in solution is influenced by the balance of  $\pi$ - $\pi$  interactions between the adjacent perylene cores and interactions with the solvent. The UV/Vis spectra of BDPPP were therefore recorded in chloroform, toluene and THF to characterise the effect of solvent polarity on the self-assembly behaviour of this system (Figure 1).

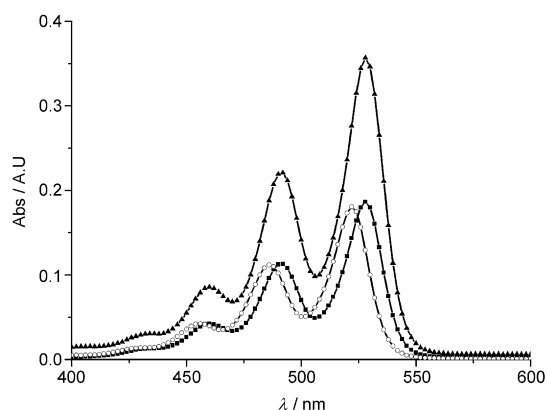


**Figure 1.** UV/Vis absorption spectra of BDPPP in organic solvents of varying polarity,  $c = 5 \times 10^{-6}$  M. ■: CHCl<sub>3</sub>; ○: THF; ▲: toluene.

Characteristic perylene absorption bands corresponding to the  $S_0$ - $S_1$  electronic transition are present between  $\lambda = 400$  and 600 nm for BDPPP in all three solvents.<sup>[24]</sup> Identical absorption maxima were obtained in CHCl<sub>3</sub> and toluene at  $\lambda = 527$ , 491 and 460 nm for the  $S_{0-0}$ ,  $S_{0-1}$  and  $S_{0-2}$  vibronic transitions, respectively.<sup>[27]</sup> In THF the absorption maxima are redshifted to  $\lambda = 522$ , 486 and 455 nm, respectively, for the equivalent transitions. The coupling of the breathing vibration of the perylene skeleton with the  $S_{0-1}$  transition polarised along the long axis of the molecule results in a clearly defined vibronic structure in the spectrum. The pattern of absorbance in these spectra is indicative of BDPPP in the molecularly dissolved form.<sup>[28]</sup> For each solvent assayed, increasing the concentration from  $10^{-6}$ – $10^{-4}$  M had little effect on the spectral features other than an enhancement of the absorption intensity, which indicated the presence of predominantly monomeric forms of BDPPP in solution throughout the investigated concentration range.

The ratio of the  $S_{0-0}$  and  $S_{0-1}$  absorptions can be used to provide insight into the degree of aggregation in solution.<sup>[29]</sup> Monomeric PDI molecules exhibit normal Frank–Condon progression with a ratio of the lowest energy absorbances  $A_{0-0}/A_{0-1}$  approximately equal to 1.6. With increasing aggregation this value decreases until it reaches a limiting value of  $\sim 0.7$ . Analyses of the  $A_{0-0}/A_{0-1}$  ratios for BDPPP confirm the observed lack of aggregation with increasing concentration (see Table 1).

CD measurements for BDPPP in solution exhibited very small positive Cotton effects in the region corresponding to the main perylene chromophore absorption which is indicative of very little induced chirality for this building block (see the Supporting Information, Figure S8b). The lack of chiral signal is to be expected for the BDPPP systems in these solvents, as

Table 1. $A_{0-0}/A_{0-1}$ ratios for BDPPP as a function of concentration in different solvents.			
$A_{0-0}/A_{0-1}$ [M]	CHCl <sub>3</sub>	Toluene	THF
$5 \times 10^{-6}$	1.68	1.64	1.64
$4 \times 10^{-5}$	1.62	1.61	1.5
$1 \times 10^{-4}$	1.46	1.44	1.32

UV/Vis measurements demonstrated that the PDI molecules were molecularly dissolved and that little aggregation was occurring.

As BTPPP exhibited poor solubility in apolar organic solvents, the aggregation properties of BTPPP were characterised by UV/Vis spectroscopy in DMSO, MeOH and water (Figure 2).

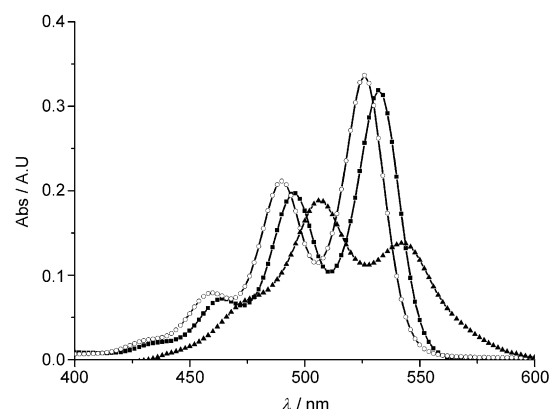


**Figure 2.** UV/Vis absorption spectra for BTPPP in DMSO, MeOH and water,  $c = 7.5 \times 10^{-6}$  M. ■: DMSO; ○: MeOH; ▲: water.

Characteristic perylene absorption bands with vibrational structure corresponding to the  $S_{0-0}$ ,  $S_{0-1}$ ,  $S_{0-2}$  and  $S_{0-3}$  transitions were clearly identified in the spectra recorded in DMSO and MeOH. In MeOH the first three transitions occur at  $\lambda = 525$ , 489 and 459 nm, respectively, with the higher energy  $S_{0-3}$  transition appearing as a low intensity shoulder at approximately 430 nm. A similar spectral pattern was observed in DMSO. The  $S_{0-0}$  transition occurs with the highest intensity in DMSO and MeOH, indicative of molecularly dissolved PDIs in these solvents. The ratios of the absorption for the  $S_{0-0}$  and  $S_{0-1}$  transitions (Table 2) are very close to the literature value of 1.6 for monomeric PDIs in solution. The large decrease in the absorption ratio in MeOH with increased concentration indicates a greater tendency for aggregation in this solvent compared

Table 2. $A_{0-0}/A_{0-1}$ ratios for BTPPP as a function of concentration in different solvents.			
$A_{0-0}/A_{0-1}$ [M]	DMSO	MeOH	Water
$5 \times 10^{-6}$	1.58	1.71	0.76
$5 \times 10^{-5}$	1.58	1.52	0.63
$4 \times 10^{-4}$	1.57	1.37	N/A <sup>[a]</sup>

[a]  $4 \times 10^{-4}$  M was not assayed for BTPPP in water due to aggregation.

with DMSO. The values in DMSO remained relatively constant in the same concentration range and little decrease in the absorption ratio occurs with increasing concentration.

In contrast to these observations, a very different spectral pattern is obtained for BTPPP in water. The absorption maximum now occurs for the  $S_{0-1}$  transition instead of the  $S_{0-0}$ , and the  $S_{0-2}$  band at  $\lambda = 475$  nm is also enhanced relative to the  $S_{0-0}$  transition. Spectral features such as these are typical of PDIs in the aggregated state. Spectra indicative of monomeric species were not observed in water even at very low concentration ( $10^{-6}$  M).  $A_{0-0}/A_{0-1}$  ratios of 0.76 and 0.63 were calculated from the UV spectrum (Table 2), which is evidence for strongly aggregated PDI molecules (the extent of which increases with concentration).

The differences in spectral features for BTPPP in aqueous solution are due to electronic coupling of the chromophores as a result of  $\pi$ - $\pi$  stacking in solution. At all concentrations assayed the absorption maxima of BTPPP are shifted to lower wavelengths in water relative to MeOH and DMSO. The hypsochromic shift of the absorption maximum in aqueous solution is characteristic of aggregates of PDIs in which the central perylene units are stacked co-facially, that is, H-aggregates.<sup>[26b,30]</sup> Aggregation most likely occurs because of the amphiphilic nature of BTPPP; the hydrophobic central units are poorly solubilised by the polar solvent and hence favour stacking to maximise hydrophobic and  $\pi$ - $\pi$  interactions.<sup>[27,31]</sup> The charged groups at the periphery enable favourable interactions with the solvent.

CD spectroscopy was used to probe the supramolecular chirality of the aggregated BTPPP perylene chromophore in solution (Figure 3). Spectra measured in water (a poor solvent for BTPPP) exhibited an induced bisignate Cotton effect between  $\lambda = 450$  and 650 nm at all concentrations assayed, which indicates that the PDI molecules aggregate in water to form helical supramolecular structures. The bisignate (negative to positive) signal with maxima occurring at  $\lambda = 510$  and 575 nm observed here is characteristic of supramolecular ordering in which the transition dipoles are arranged in a right-handed or clockwise helical orientation (P helicity).<sup>[32]</sup>

In DMSO and MeOH (good solvents), very low intensity positive Cotton effect signals occurred in the region of perylene

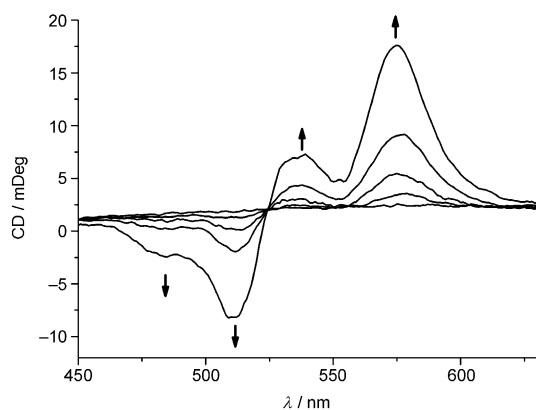


Figure 3. CD spectra of BTPPP ( $2.5 \times 10^{-6}$ – $5 \times 10^{-5}$  M) in aqueous solution at room temperature. Arrows indicate changes upon increasing concentration.

absorption at low concentration (up to  $5 \times 10^{-6}$  M). These signals were similar to that observed for BDPPP in THF,  $\text{CHCl}_3$ , and toluene. To investigate the concentration-dependent self-assembly properties of BTPPP, further CD measurements were taken at a higher range of concentrations ( $7.5 \times 10^{-5}$ – $4 \times 10^{-4}$  M, Supporting Information, Figure S9a,b) in MeOH and DMSO. The  $A_{0-0}/A_{0-1}$  ratios obtained for BTPPP by UV/Vis indicated increased aggregation with increased concentration in MeOH. CD results obtained at higher concentration were in good agreement with this observation, with a transition from molecularly dissolved to supramolecular aggregates observed for BTPPP in MeOH. At  $4 \times 10^{-4}$  M a bisignate Cotton effect centred on the absorption maximum of the  $S_{0-0}$  transition emerged for BTPPP in MeOH, indicative of right-handed helical architectures as observed in water. The higher threshold concentration required for ordered aggregation in MeOH vs. water is attributed to the increased ability of MeOH to solvate individual molecules of BTPPP (as seen from  $A_{0-0}/A_{0-1}$  ratios). Similar effects were not observed for DMSO, which retained its ability to solvate BTPPP very well in the concentration range assayed (also reflected by  $A_{0-0}/A_{0-1}$  ratios in Table 2).

To obtain further information on the aggregation behaviour of BTPPP, fluorescence spectra were recorded. At  $5 \times 10^{-5}$  a well-defined emission spectrum is observed for BTPPP in MeOH (Figure 4), with two highly resolved emission peaks ob-

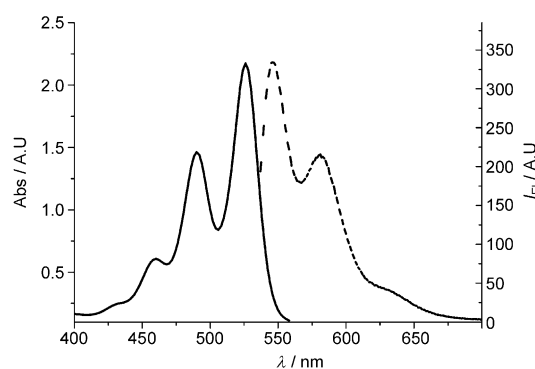


Figure 4. Mirror-image UV/Vis/fluorescence spectra for BTPPP in MeOH  $c = 5 \times 10^{-5}$  M, (excitation at 470 nm, slit width = 2.5 nm).

served in the range  $\lambda = 500$ –650 nm. The emission spectrum is the mirror image of the UV/Vis absorption spectrum, with a Stokes shift of 25 nm. Spectra such as these are characteristic of PDI systems in which little or no aggregation is occurring.<sup>[33]</sup>

To gain further insight, the concentration-dependent fluorescence of BTPPP was recorded in MeOH and aqueous solution (ESI, Figure S10a and b, respectively). In contrast to spectra obtained in MeOH, the emission spectra of BTPPP obtained in aqueous solution do not exhibit mirror image symmetry with the corresponding UV/Vis spectra. Large Stokes shifts were observed relative to the molecular dissolved spectrum in MeOH. Emission spectra such as these are typical for PDI systems in which H-aggregation is occurring.<sup>[34]</sup>

Similar overall trends occur in the concentration-dependent emission intensity for BTPPP in both MeOH and aqueous solu-

tion (Figure S10.1, Supporting Information). The spectra are characterised by an initial increase in fluorescence intensity with concentration until a threshold concentration is reached ( $1 \times 10^{-4}$  M in MeOH and  $5 \times 10^{-5}$  M in water). Above this value, further increases in concentration result in strong fluorescence quenching. It has been reported previously for H-aggregated PDI systems that a broad structureless emission band corresponding to the aggregated species emerges at high concentration,<sup>[35]</sup> no such spectral features were observed for BTPPP in the concentration range assayed here. Instead, the emission maxima undergo a reversal in fluorescence intensity with increasing concentration; the higher energy emission band is redshifted from  $\lambda = 556$  to 604 nm in water, and  $\lambda = 540$  to 554 nm in MeOH, with concurrent broadening of spectra and loss of vibronic fine structure. Similar changes in emission intensity reversal have been reported for PDI dimer systems.<sup>[36]</sup> The lower threshold concentration for fluorescence quenching for BTPPP in water is indicative of the increased tendency for aggregation in this solvent vs. MeOH (as already seen from  $A_{0-0}/A_{0-1}$  ratios). By  $4 \times 10^{-4}$  M a broad structureless redshifted emission band occurs for BTPPP in water. In contrast, some vibronic structure persists in the spectra obtained in MeOH at this concentration.

The concentration-dependent fluorescence results obtained in MeOH are in good agreement with the UV/Vis and CD spectra obtained for BTPPP, which indicated a transition from the monomeric to ordered chiral aggregates in this same concentration interval ( $1 \times 10^{-4}$  M). It is likely that the loss in fluorescence is due to aggregation-induced quenching.<sup>[28a,37]</sup> UV/Vis spectra for BTPPP in aqueous solution demonstrated the formation of PDI aggregates from concentrations as low at  $10^{-6}$  M. It is therefore unlikely that the change in the fluorescence intensity observed is due to the onset of aggregation in aqueous solution. Instead, it is possible that the change in emission intensity above the threshold concentration is due to an aggregate structural change (either in the ground or excited state) leading to new pathways for fluorescence quenching. This structural reorganisation most likely results in increased  $\pi$ - $\pi$  interactions and excitonic coupling (as evidenced in the spectra by line broadening). These new pathways most probably represent self-quenching mechanisms as a result of intermolecular interactions by the higher ordered aggregates at increased concentration.<sup>[26a,35,38]</sup> Fluorescence lifetime and quantum yield measurements might provide further information on the fluorescence properties and nature of the PDI aggregates at increased concentration.

### Temperature and concentration-dependent aggregation

To investigate aggregate formation and determine the mode of self-assembly of BTPPP, temperature-dependent UV/Vis and CD measurements were carried out in aqueous solution (Figure 5). Temperature-dependent UV/Vis spectra of BTPPP exhibited an increase in the absorption intensity as well as a gradual reversal in the intensity of the  $S_{0-0}$  to  $S_{0-1}$  absorption maxima with increasing temperature.

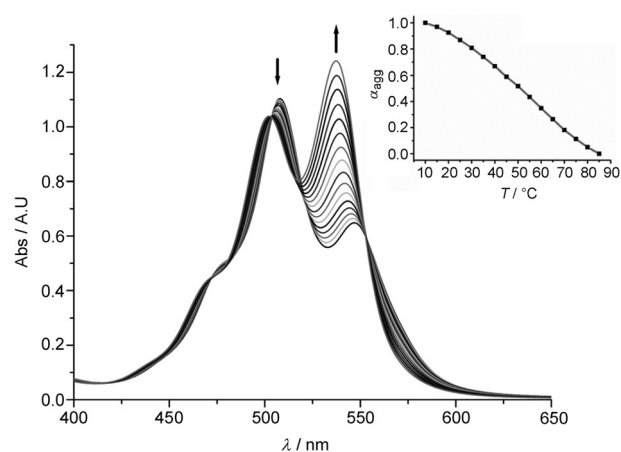


**Figure 5.** Variable temperature UV/Vis absorption of BTPPP in H<sub>2</sub>O from 10–85 °C ( $5 \times 10^{-5}$  M). Arrows indicate changes upon increasing temperature. Degree of aggregated molecules  $\alpha_{\text{agg}}$  as a function of temperature for BTPPP in H<sub>2</sub>O is shown in the inset (■: BTPPP).

These spectral features are indicative of the transition from aggregated to molecularly dissolved species as a function of temperature. The UV/Vis spectrum obtained at the highest temperature of 85 °C exhibits similarities to that observed for molecularly dissolved BTPPP in DMSO. Isobestic points occur at 472, 503 and 552 nm, which indicates a transition from aggregated to monomeric species. The temperature-dependent CD spectrum of BTPPP in water also exhibits a transition to the molecularly dissolved species with increasing temperature (Figure 6). The bisignate Cotton effect corresponding to right-handed helical aggregates diminishes with increasing temperature; when 85 °C is reached, no Cotton effect is observed.

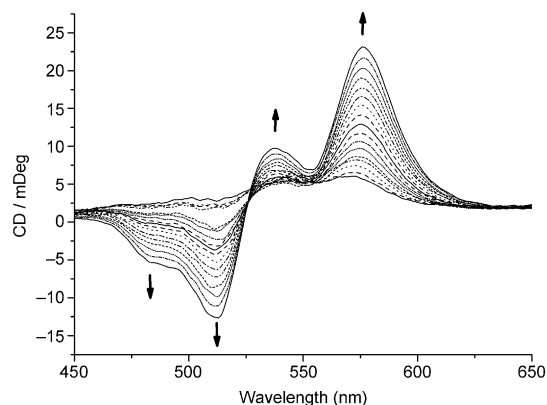


**Figure 6.** Temperature-dependent CD spectra of BTPPP in H<sub>2</sub>O from 5–85 °C ( $5 \times 10^{-5}$  M). Arrows indicate the changes upon decreasing temperature.

Planar discotic molecules such as PDIs commonly self-assemble in solution to give open-ended 1D columnar aggregates.<sup>[3]</sup> This process is driven by  $\pi$ - $\pi$  interactions between the aromatic cores, which stack with a spacing of approximately 0.34 nm. Such self-assembly behaviour can be described by the equal  $K$  or isodesmic model,<sup>[39]</sup> in which aggregation occurs in a step-

wise fashion without a change in the equilibrium constant  $K$ .<sup>[40]</sup> Temperature-dependent UV/Vis measurements were used to calculate the variance in the mole fraction of aggregate with temperature ( $\alpha_{\text{agg}}(T)$ ) according to Equation (1):

$$\alpha(T) \approx \frac{A(T) - A_{\text{mon}}}{A_{\text{agg}} - A_{\text{mon}}} \quad (1)$$

The values at each temperature were taken at  $\lambda_{\text{max}} = 508$  nm with  $A_{\text{mon}}$  and  $A_{\text{agg}}$  corresponding to the extinction coefficients for the molecularly dissolved and fully aggregated species, respectively (see the Supporting Information Figure S11 for further details). The change in mole fraction of aggregates as a function of temperature for BTPPP could be fitted very well to a sigmoidal curve (Figure 5, inset) typical of systems in which an isodesmic model of self-assembly is occurring, and illustrates that the aggregation of the PDI in aqueous solution is well described by this model.<sup>[32b,41]</sup> The isodesmic model for aggregation has been successfully demonstrated for many other PDI systems.<sup>[28b,38,42]</sup> The similarity in the pattern of the cooling spectra (Figure 6) and CD spectra obtained at RT (Figure 3) is indicative of reversible aggregation, a feature typical of systems employing an isodesmic mode of self-assembly.<sup>[3,26a]</sup> Assuming an isodesmic model of self-assembly for BTPPP in aqueous solution, the melting temperature (the temperature at which  $\alpha(T) = 0.5$ ) and the average stack length of the aggregates ( $DP_N$ ) can be calculated according to Equations (1) and (2):

$$DP[T] = \frac{1}{\sqrt{1 - \alpha(T)}} \quad (2)$$

From Equation (1), the melting temperature was determined as 55 °C for BTPPP at  $5 \times 10^{-5}$  M from the isodesmic plot (inset Figure 5). The reversal in the absorption maxima from  $S_{0-0}$  to  $S_{0-1}$  can be seen at this temperature (Figure 5), representative of the transition from the aggregated to the monomeric forms of BTPPP. Values obtained for the average stack length of BTPPP at variable temperatures and concentration (from Equation 2) are shown in Table 3. The stack length increases linearly with concentration at both 25 and 60 °C over the range  $1-5 \times 10^{-5}$  M (Table 3 and Figure S12 in the Supporting Information). Relatively small changes in the average stack length occur over this concentration with predominantly dimer and trimer spe-

Table 3. $A_{0-0}/A_{0-1}$ Degree of aggregated molecules and average number of aggregated molecules $DP_N$ for BTPPP as a function of temperature and concentration in H <sub>2</sub> O.				
Concentration [M]	$T_m$ [°C] <sup>[a]</sup>	$\alpha_{\text{agg}}$ <sup>[b]</sup>	$DP_N$ <sup>[c]</sup>	$DP_N$ <sup>[d]</sup>
$5 \times 10^{-5}$	55	0.59	3.0	1.32
$3 \times 10^{-5}$	–	0.42	2.76	1.21
$1 \times 10^{-5}$	–	0.39	2.45	1.12

[a]  $T_m$  = melting temperature of aggregates (at  $\alpha_{\text{agg}} = 0.5$ ). [b] Values determined at 50 °C. [c] Values determined at 25 °C. [d] Values determined at 60 °C.

cies observed. These changes indicate isodesmic self-assembly, in which the increase in stack length of the self-assembled aggregates occurs relatively slowly, with larger-sized aggregates only observed at higher concentrations.<sup>[43]</sup> At  $5 \times 10^{-5}$  M, an overall decrease in the average stack length is observed with increasing temperature for BTPPP, with an average stack length of  $\sim 3$  occurring at 25 °C. Previously reported  $DP_N$  values for core-substituted PDIs have been as high as 38.<sup>[44]</sup> It is likely that the bulky substituents within the side chains reduce the propensity for stacking in solution, leading to the lower  $DP_N$  values obtained for BTPPP.

### Solid-state characterization of thin films

To investigate the aggregation properties of BTPPP in the solid state, thin films cast from MeOH, DMSO and aqueous solution were analysed by CD and UV/Vis spectroscopy. Films were prepared by casting solutions ( $1 \times 10^{-4}$  M) onto quartz slides and allowing the solvent to evaporate slowly in air. All films cast from the different solvents gave very similar UV/Vis absorption spectra (inset, Figure 7a). The spectra appear broadened relative to those obtained in solution, and the absorption maximum of highest intensity occurs for the  $S_{0-1}$  transition. The blueshift of the absorption maximum relative to the monomer-

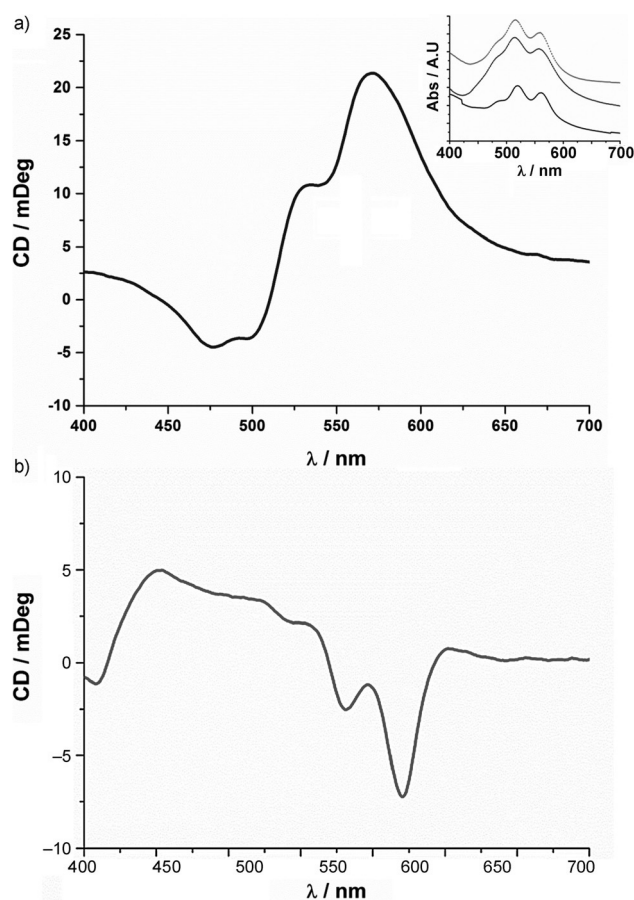


Figure 7. a) CD spectrum of BTPPP film cast from H<sub>2</sub>O. Inset: UV/Vis spectra of films of BTPPP cast from various solvents (—: MeOH; ----: DMSO; .....: H<sub>2</sub>O). b) CD spectrum of BTPPP film cast from MeOH.

ic species is characteristic of H-aggregates of the PDI units in which the transition dipoles are eclipsed.<sup>[45]</sup> Further investigation into the packing features of the aggregates in the films was carried out using CD spectroscopy. Films cast from DMSO and water gave CD spectra characteristic of BTPPP in aqueous solution (see Figure 3 and Figure 7b). A bisignate absorption occurred in the region of the perylene chromophore corresponding to the arrangement of the perylene chromophores of BTPPP in a right-handed helical fashion.<sup>[25,46]</sup>

The intensity of the Cotton effects were diminished, with respect to that occurring in solution, likely due to increased excitonic coupling between the perylene aggregates in thin films. The similarity in the CD spectra obtained for BTPPP in solution and solid-state films indicates that the molecular packing features in solution are conserved for BTPPP in thin films cast from water solvent.

In contrast to DMSO and water, thin films cast from MeOH indicated the formation of left-handed helical architectures (Figure 7a). This observed effect was opposite to the right-handed helical aggregates observed at high concentration in MeOH solution. Helical bias is often due to the energetic difference between the right- and left-handed conformations; this can originate from steric hindrance imparted by chiral groups located at peripheral positions in the molecular building blocks.<sup>[15b]</sup> It has been demonstrated previously for PDI materials that the self-assembled structure can be tuned by modifying external factors such as temperature<sup>[16]</sup> and solvent.<sup>[47]</sup> These conditions can be used to establish non-equilibrium conditions, thus enabling control over kinetic or thermodynamic pathways of self-assembly to obtain structures of desired helicity.<sup>[48]</sup> Factors that promote a fast aggregation rate, such as rapid cooling and high concentration, can lead to self-assembly processes that occur by a kinetically controlled pathway.<sup>[49]</sup> This behaviour has been demonstrated recently by investigations in which tuneable helicity of PDI materials was achieved by employing non-equilibrium conditions using solvent,<sup>[17]</sup> ultrasound,<sup>[36b,50]</sup> and concentration.<sup>[51]</sup> It is likely that the formation of left-handed helical aggregates occurs by a kinetically controlled pathway for BTPPP films cast from MeOH. It is proposed that the lower boiling point of MeOH results in a faster rate of evaporation for films cast from this solvent in comparison with DMSO and water. Under these conditions, aggregation occurs more rapidly and a reduced equilibration time leads to the formation of left-handed helical architectures by a kinetic pathway. UV/Vis and CD measurements of BTPPP in DMSO, MeOH and aqueous solution all exhibited right-handed helical architectures in both concentration and temperature-dependent (in aqueous solution) methods, providing strong evidence that the right-handed helical orientation of BTPPP is the thermodynamically stable confirmation.

TEM was used to image films prepared from solution, and revealed self-assembled structures for BTPPP from MeOH, H<sub>2</sub>O and DMSO (Figure 8 and Figure S12.1 in the Supporting Information). Films were prepared from solutions of higher ( $4 \times 10^{-4}$  M) and lower concentration ( $2.5 \times 10^{-5}$  M) to investigate the effect of concentration on the observed structures. Films cast from  $2.5 \times 10^{-5}$  M aqueous solution are shown in Figure 8a.

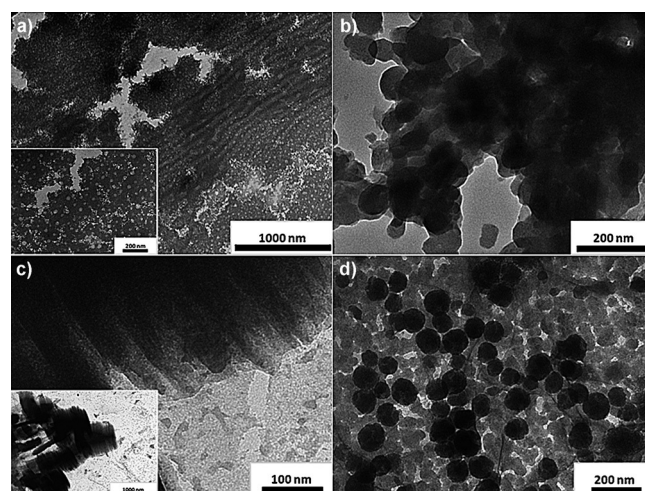


**Figure 8.** TEM images of BTPPP cast from solvents of different concentration: a) aqueous solution,  $2.5 \times 10^{-5}$  M; b) aqueous solution,  $4 \times 10^{-4}$  M; c) DMSO,  $2.5 \times 10^{-5}$  M; d) DMSO,  $4 \times 10^{-4}$  M.

Self-assembly of BTPPP in aqueous solution of low concentration resulted in a porous sheet-like structure. Closer examination of the sheet revealed a layered arrangement with evidence of wire-like morphology on a smaller scale. Self-assembly of these wire-like structures give nanofibrillar architectures on a larger length scale. In contrast to the structures obtained at low concentration, films cast from aqueous solution of higher concentration yielded disordered globular morphologies (Figure 8b).

As spectroscopic studies indicated that DMSO was a good solvent for BTPPP, self-assembly in this solvent was likely to occur from the interaction of molecularly dissolved PDI monomers as the concentration increased. Films cast from DMSO solution of low concentration ( $2.5 \times 10^{-5}$  M) exhibited nanosheet-like structures (Figure 8c). In contrast to aggregates of wires found in aqueous solution, thin continuous plate-like nanoribbons of finite size were formed from DMSO (Figure 8c). Films prepared from DMSO solution of higher concentration gave predominantly spherical aggregates approximately 100 nm in diameter (Figure 8d), similar to those formed in aqueous solution at higher concentration. In contrast, structures with very little ordering were observed in films cast from MeOH at low concentration. Films cast from MeOH at higher concentration exhibited a mixture of disordered aggregates and nanofiber morphologies (see Figure S12.1 in the Supporting Information). It is noteworthy that none of the conditions employed here produced structures that reflected the chirality observed from solution studies, most likely due to the presence of very short aggregate stacks (Table 3).

### Structural and mesophase characterization

XRD was used to obtain information of the molecular organisation of BDPPP and BTPPP in the solid state. The absence of a clearing temperature before onset of degradation prevented the preparation of thermally annealed samples of the materials for X-ray analysis. Bulk samples of both BDPPP and BTPPP ex-

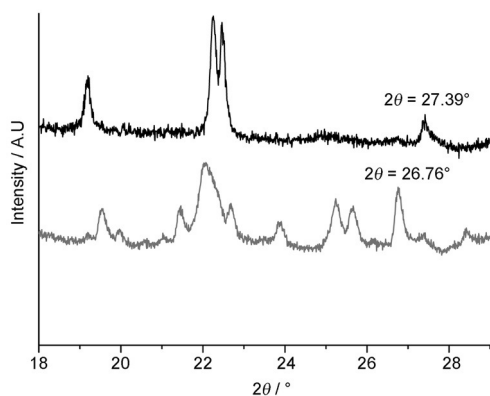


**Figure 9.** Wide-angle X-ray diffraction pattern for bulk samples of BDPPP (—) and BTPPP (---).

hibit multiple sharp diffraction peaks in the wide-angle region indicative of their highly crystalline character (Figure 9). Generally, the planar geometry of PDIs promotes the formation of columnar assemblies by way of  $\pi$ - $\pi$  interactions between the central perylene units. Typical  $\pi$ -stacking distances for conjugated dye materials are of the range 3.3–4 Å.<sup>[52]</sup> BDPPP exhibited a sharp reflection of high intensity at  $2\theta = 26.76^\circ$ , corresponding to a  $\pi$ - $\pi$  intra-columnar spacing of 3.3 Å, characteristic of perylene diimide materials.<sup>[53]</sup> For BTPPP the  $\pi$ - $\pi$  stacking reflection occurs at  $2\theta = 27.39^\circ$  giving a smaller  $\pi$ - $\pi$  stacking distance of 3.26 Å. Although the charged and bulky trimethylammonium groups are present in the case of BTPPP, and lead to a broader and lower intensity stacking reflection, it does not hinder the formation of stacked PDI aggregates. Both PDI building blocks also exhibit a number of reflections centred around  $2\theta \sim 22^\circ$  ( $\sim 4$  Å).<sup>[44]</sup>

The anisotropic structural features of BTPPP and BDPPP (with two axes much larger than the third) are similar to that of discotic mesogens. The combination of flexible side chains at the periphery and possibilities for  $\pi$ -stacking interactions favour mesophase formation; hence the liquid-crystalline properties of the perylene diimide building blocks were investigated. Differential scanning calorimetry (DSC), and polarising optical microscopy (POM) were used to ascertain whether any lyotropic or thermotropic liquid-crystal phases occurred for the materials. DSC was carried out on the as-prepared materials; PLM investigations were performed into solvent annealed films prepared from DMSO and acetonitrile.

DSC thermograms were obtained for both PDIs in the as-prepared form, with no phase transitions observed for BTPPP. For BDPPP, DSC measurements indicated reversible transitions centred at 107 and 147 °C in the cooling and heating curves, respectively (Figure 10). The transition in the heating curve is relatively broad, with an enthalpy value of  $\Delta H = 2.7$  kJ mol<sup>-1</sup>. Typical enthalpy values for the transition from the crystalline to the mesophase fall in the range of 30–50 kJ mol<sup>-1</sup>.<sup>[54]</sup> The lower enthalpy value obtained for this transition indicates that it is likely to correspond to a crystal-crystal structural rearrangement. Additionally, transitions of significantly smaller enthalpy were also observed (196 and 251 °C) in the cooling and

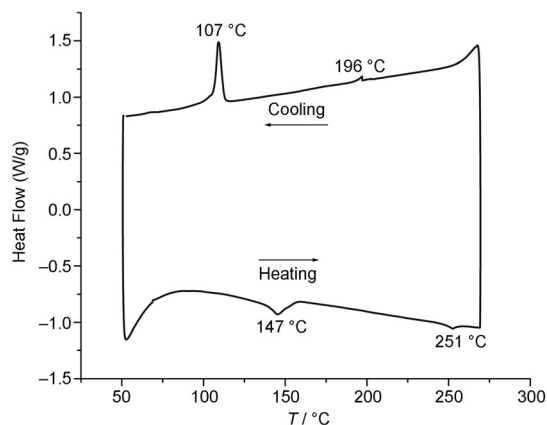


**Figure 10.** DSC thermogram for BDPPP, first cooling, second heating curves; as-prepared material.

heating curves, respectively. All transitions observed by DSC were investigated in further detail by temperature-dependent polarised optical microscopy (POM).

POM investigations into the as-prepared materials did not reveal any characteristic thermotropic textures at room temperature, which fitted with the crystalline nature as found by XRD (see Figure S13 in the Supporting Information). Observation of BDPPP using the same temperature conditions employed in the DSC investigations exhibited no visible changes at the observed transition temperatures, providing further evidence that these transitions corresponded to minor structural rearrangements.

Subsequently, attempts were made to characterise the mesophase properties of BTPPP by solvent annealing with DMSO. Films cast from DMSO were annealed at 75 °C and observation by POM revealed fan-shaped textures characteristic of ordered columnar mesophases. Heating and cooling of these films (up to 100 °C) did not reveal any phase changes. Samples of BTPPP were prepared from acetonitrile (a good solvent for the charged PDI) by peripheral evaporation under the microscope. These gave spherulitic textures with distinct maltose crosses typical of columnar liquid-crystalline phases (Figure 11b).<sup>[44]</sup> It is suggested that the absence of soft plasticizing alkyl tails around the rigid and crystalline PDI cores contributes to the absence of any further mesophases. ISA therefore provides an excellent opportunity to add a range of alkyl tails through surfactant complexation, thus providing opportunities for the formation of mesophases.

## Conclusions

A chiral PDI, intended for use as a novel tecton in the production of ionic self-assembled materials, was successfully synthesised. The amphiphilic nature of the charged moiety, BTPPP, enabled its aggregation behaviour to be selectively controlled by rational choice of solvent, concentration and temperature. The molecular chirality of the side chains was translated into a chiral supramolecular structure in the form of right-handed helical aggregates in aqueous solution, as very clearly shown by concentration-dependent CD studies. Such expression of

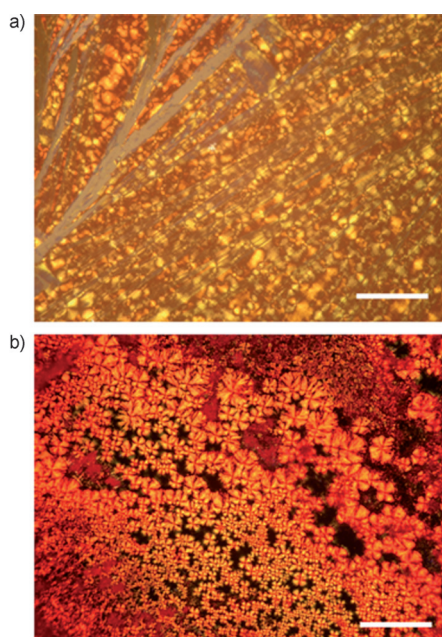


**Figure 11.** POM images of BTPPP: a) Solvent-annealed film from DMSO b) prepared by peripheral evaporation from acetonitrile, scale bar = 50  $\mu\text{m}$ .

molecular chirality was not observed for the uncharged precursor BDPPP. Temperature-dependent UV/Vis and CD studies were used to follow the transition to the molecularly dissolved phase at elevated temperatures; this process is reversible, as indicated by the nearly identical gradient of the temperature-dependent spectra obtained from CD spectroscopy. The UV/Vis data was fitted to an isodesmic model of assembly, and stack lengths of aggregates were calculated, with  $DP_N \leq 3$ . It is suggested that the short-stack lengths contributed to the fact that no clear expression of the molecular chirality was found in either the poorly defined solid-state aggregates or in the observed mesophase structures. The solvent processibility of these materials, in combination with the ability to induce chirality into the supramolecular structures formed in solution makes these PDIs highly desirable candidates for the preparation of complex anisotropic materials by ionic self-assembly.

## Experimental Section

### Materials and methods

$^1\text{H}$  NMR spectra were recorded on JEOL spectrometers (Lambda 300 and Eclipse 400 at 300 and 400 MHz, respectively) and referenced to deuterated solvents. CD measurements were obtained with a JASCO-J815 spectropolarimeter fitted with a Peltier temperature controller. UV/Vis data was recorded using a PerkinElmer Lambda 35 UV/Vis spectrometer in the range 200–800 nm with a Peltier temperature controller. For UV and CD spectra recorded with temperature, heating was carried out at a rate of  $60^\circ\text{C h}^{-1}$ . Fluorescence measurements were obtained using a Varian Cary spectrophotometer at an excitation wavelength of  $\lambda = 470$  nm in the range  $\lambda = 500$ –800 nm. Due to the high-emission intensity of samples, slit widths of  $\lambda = 2.5$  and 5 nm was used for MeOH and aqueous solutions respectively. All spectra were ob-

tained at RT unless otherwise specified, standard 1 mm or 10 mm path quartz cuvettes were used depending on sample concentration. 10 mm path length cuvettes were used for all spectroscopic investigations unless specified otherwise. Quartz slides were used for thin film spectroscopic measurements. TGA was carried out on a Perkin–Elmer STA6000 simultaneous thermal analyser with an internal microbalance and thermocouple. DSC analyses were performed on Q100 from TA instruments coupled to a refrigerated cooling system (RCS90) at a scanning rate of  $10^\circ\text{C min}^{-1}$ . The sample holders used were nonhermetic aluminium pans, and the sample weight was obtained using a XT220A Precisa microbalance. TEM was performed on a JEOL 1200EX TEM MK2 with a tungsten filament at an operating frequency of 120 kV. The instrument is equipped with a MegaView II digital camera using Soft Imaging Systems 3.0 image software. Samples were prepared by dropcasting onto carbon-coated copper grids on Teflon film and set to dry under ambient conditions unless otherwise stated. XRD (WAXS) data was recorded with  $\text{Cu}_{K\alpha}$  radiation ( $\lambda = 1.5418$  Å) on a Bruker D8 advance powder diffractometer fitted with a 0.6 mm fixed divergence slit, knife-edge collimator and a LynxEye detector. POM images were obtained using a Nikon BX-50 microscope fitted with an Olympus C-5060 wide zoom digital camera. Films prepared by solvent annealing from DMSO were dried at  $75^\circ\text{C}$  for 12 h. BTPPP samples prepared from acetonitrile for POM were of unknown concentration.

### General procedure for the synthesis of *N,N'*-bis[2-(dimethylamino)-3-(phenyl)propyl]perylene diimide

Perylene tetracarboxylic dianhydride (44 mg, 0.112 mmol) and *N,N'*-dimethylamino-3-phenylpropanamine (100 mg, 0.56 mmol) were dissolved in butan-1-ol (8 mL). This mixture was heated to  $90^\circ\text{C}$  under nitrogen for 24 h. TLC analysis indicated a reaction had occurred. ( $\text{CHCl}_3/\text{BuOH}$  10:1, triethylamine). The solvent was removed by evaporation under reduced pressure, and the product washed with stirring in NaOH (aq) (5% w/v) for 30 m at  $90^\circ\text{C}$ . The solid product was obtained by centrifugation, then washed with stirring in a EtOH/water solvent (3:1 w/v). The product was obtained by centrifugation and dried under vacuum and used without further purification. Yield: 61 mg, 76.5%;  $^1\text{H}$  NMR (300 MHz,  $\text{CDCl}_3$ ):  $\delta = 8.6$ –8.53 (m, 8H,  $\text{H}_{\text{PERY}}$ ), 7.26–7.00 (m, 10H,  $\text{H}_{\text{PHE}}$ ), 4.46 (dd, 2H,  $J = 13.3$ , 8.6 Hz, C(1) $\text{H}_{2a}$ ), 4.14 (dd, 2H,  $J = 13.3$ , 6.3 Hz, C(1) $\text{H}_{2b}$ ), 3.67–3.62 (m, 2H, C(2)H), 3.09 (dd, 2H,  $J = 14.0$ , 4.6 Hz, C(3) $\text{H}_{2a}$ ), 2.60 (dd, 2H,  $J = 14.0$ , 9.2 Hz, C(3) $\text{H}_{2b}$ ), 2.44 ppm (s, 12H,  $\text{CH}_3$ ); MS (ESI $^+$ ):  $m/z$ : 713.1 [ $M+H$ ] $^+$

### General Procedure for the synthesis of *N,N'*-bis[2-(trimethylammonium)-3-(phenyl)propyl]perylene diimide

*N,N'*-Bis[2-(dimethylamino)-3-(phenyl)propyl]perylene diimide (BDPPP, 30 mg, 0.042 mmol) was dissolved in DMF (2 mL) and methyl iodide (0.262 mL, 4.2 mmol) was added. Additional DMF (2 mL) was added and the mixture was stirred under an inert nitrogen atmosphere at  $30^\circ\text{C}$  for 24 h, then at RT for a further 12 h. TLC analysis was used to monitor the reaction progress ( $\text{CHCl}_3/\text{EtOH}$ , triethylamine 10:3). The solvent was removed by evaporation at reduced pressure to give the product, a dark purple solid. The product was washed with stirring in chloroform (50 mL) for 1 h. The bright pink solvent was removed by decantation and the solid sample dried under vacuum. Yield: 26.8 mg, 64%;  $^1\text{H}$  NMR (300 MHz,  $\text{CD}_3\text{CN}$ ):  $\delta = 8.64$ –8.39 (m, 8H,  $\text{H}_{\text{PERY}}$ ), 7.12–6.66 (m, 10H,  $\text{H}_{\text{PHE}}$ ), 4.83 (dd, 2H,  $J = 13.3$ , 8.5 Hz, C(1) $\text{H}_{2a}$ ), 4.54 (dd, 2H,  $J = 13.3$ , 4.7 Hz, C(1) $\text{H}_{2b}$ ), 4.50–4.42 (brm, 2H, C(2)H), 3.51–3.44 (brm, 2H,

C(3)H<sub>2a</sub>), 3.35 (s, 18H, CH<sub>3</sub>), 3.06–3.01 ppm (br m, 2H, C(3)H<sub>2b</sub>); MS (ESI<sup>+</sup>): *m/z*: 371.18 [M]<sup>2+</sup>

## Acknowledgements

G.E. thanks the EPSRC for support. G.C.L.J. was a Royal Society Wolfson Research Merit Award Holder during the period this work was conducted. C.F.J.F. thanks the University of Bristol and the Bristol Centre for Functional Nanomaterials for support.

**Keywords:** chirality · chiro-optical devices · helical superstructures · perylene diimide · self-assembly

- [1] a) G. M. Whitesides, J. P. Mathias, C. T. Seto, *Science* **1991**, *254*, 1312–1319; b) I. W. Hamley, *Angew. Chem. Int. Ed.* **2003**, *42*, 1692–1712; *Angew. Chem.* **2003**, *115*, 1730–1752; c) J. M. Lehn, *Angew. Chem. Int. Ed. Engl.* **1990**, *29*, 1304–1319; *Angew. Chem.* **1990**, *102*, 1347–1362.
- [2] a) F. Würthner, *Chem. Commun.* **2004**, 1564–1579; b) X. W. Zhan, A. Facchetti, S. Barlow, T. J. Marks, M. A. Ratner, M. R. Wasielewski, S. R. Marder, *Adv. Mater.* **2011**, *23*, 268–284.
- [3] Z. J. Chen, A. Lohr, C. R. Saha-Moller, F. Würthner, *Chem. Soc. Rev.* **2009**, *38*, 564–584.
- [4] L. Schmidt-Mende, A. Fechtenkotter, K. Müllen, E. Moons, R. H. Friend, J. D. MacKenzie, *Science* **2001**, *293*, 1119–1122.
- [5] B. A. Jones, M. J. Ahrens, M. H. Yoon, A. Facchetti, T. J. Marks, M. R. Wasielewski, *Angew. Chem. Int. Ed.* **2004**, *43*, 6363–6366; *Angew. Chem.* **2004**, *116*, 6523–6526.
- [6] G. Horowitz, F. Kouki, P. Spearman, D. Fichou, C. Nogues, X. Pan, F. Garnier, *Adv. Mater.* **1996**, *8*, 242–245.
- [7] D. Görl, X. Zhang, F. Würthner, *Angew. Chem. Int. Ed.* **2012**, *51*, 6328–6348; *Angew. Chem.* **2012**, *124*, 6434–6455.
- [8] X. Sun, M. Mura, H. T. Jonkman, L. N. Kantorovich, F. Silly, *J. Phys. Chem. C* **2012**, *116*, 2493–2499.
- [9] T. Ma, C. Li, G. Q. Shi, *Langmuir* **2008**, *24*, 43–48.
- [10] a) F. Würthner, C. Bauer, V. Stepanenko, S. Yagai, *Adv. Mater.* **2008**, *20*, 1695–1698; b) S. Asir, A. S. Demir, H. Icil, *Dyes Pigm.* **2010**, *84*, 1–13.
- [11] a) R. K. Sun, C. M. Xue, M. Owak, R. M. Peetz, S. Jin, *Tetrahedron Lett.* **2007**, *48*, 6696–6699; b) X. Lu, Z. Guo, C. Sun, H. Tian, W. Zhu, *J. Phys. Chem. B* **2011**, *115*, 10871–10876; c) J. K. Gallaher, E. J. Aitken, R. A. Keyzers, J. M. Hodgkiss, *Chem. Commun.* **2012**, *48*, 7961–7963; d) M. B. Avinash, T. Govindaraju, *Adv. Mater.* **2012**, *24*, 3905–3922.
- [12] a) C. M. Xue, M. Z. Chen, S. Jin, *Polymer* **2008**, *49*, 5314–5321; b) C. D. Schmidt, C. Bottcher, A. Hirsch, *Eur. J. Org. Chem.* **2009**, 5337–5349; c) Y. Sun, C. He, K. Sun, Y. Li, H. Dong, Z. Wang, Z. Li, *Langmuir* **2011**, *27*, 11364–11371.
- [13] a) M. Wolffs, N. Delsuc, D. Veldman, N. Van Anh, R. M. Williams, S. C. J. Meskers, R. A. J. Janssen, I. Huc, A. Schenning, *J. Am. Chem. Soc.* **2009**, *131*, 4819–4829; b) E. K. Todd, S. Wang, X. H. Wan, Z. Y. Wang, *Tetrahedron Lett.* **2005**, *46*, 587–590; c) C. Thalacker, F. Würthner, *Adv. Funct. Mater.* **2002**, *12*, 209–218.
- [14] a) M. M. J. Smulders, A. Schenning, E. W. Meijer, *J. Am. Chem. Soc.* **2008**, *130*, 606–611; b) T. E. Kaiser, V. Stepanenko, F. Würthner, *J. Am. Chem. Soc.* **2009**, *131*, 6719–6732; c) J. van Gestel, A. R. A. Palmans, B. Titulaer, J. Vekemans, E. W. Meijer, *J. Am. Chem. Soc.* **2005**, *127*, 5490–5494; d) A. R. A. Palmans, E. W. Meijer, *Angew. Chem. Int. Ed.* **2007**, *46*, 8948–8968; *Angew. Chem.* **2007**, *119*, 9106–9126.
- [15] a) T. Seki, A. Asano, S. Seki, Y. Kikkawa, H. Murayama, T. Karatsu, A. Kitamura, S. Yagai, *Chem. Eur. J.* **2011**, *17*, 3598–3608; b) Y. Yang, Y. Zhang, Z. Wei, *Adv. Mater.* **2013**, *25*, 6039–6049.
- [16] V. Dehm, Z. J. Chen, U. Baumeister, P. Prins, L. D. A. Siebbeles, F. Würthner, *Org. Lett.* **2007**, *9*, 1085–1088.
- [17] J. Hu, W. Kuang, K. Deng, W. Zou, Y. Huang, Z. Wei, C. F. J. Faul, *Adv. Funct. Mater.* **2012**, *22*, 4149–4198.
- [18] a) K.-R. Wang, H.-W. An, L. Wu, J.-C. Zhang, X.-L. Li, *Chem. Commun.* **2012**, *48*, 5644–5646; b) M. M. Safont-Sempere, P. Osswald, K. Radacki, F. Würthner, *Chem. Eur. J.* **2010**, *16*, 7380–7384.
- [19] X. Feng, V. Marcon, W. Pisula, M. R. Hansen, J. Kirkpatrick, F. Grozema, D. Andrienko, K. Kremer, K. Müllen, *Nat. Mater.* **2009**, *8*, 421–426.
- [20] C. F. J. Faul, *Acc. Chem. Res.* **2014**, *47*, 3428–3438.
- [21] R. Ahmed, A. Priimagi, C. F. J. Faul, I. Manners, *Adv. Mater.* **2012**, *24*, 926–931.
- [22] R. Ahmed, S. K. Patra, I. W. Hamley, I. Manners, C. F. J. Faul, *J. Am. Chem. Soc.* **2013**, *135*, 2455–2458.
- [23] a) Y. Guan, Y. Zakrevskyy, J. Stumpe, M. Antonietti, C. F. J. Faul, *Chem. Commun.* **2003**, 894–895; b) Y. Zakrevskyy, C. F. J. Faul, Y. Guan, J. Stumpe, *Adv. Funct. Mater.* **2004**, *14*, 835–841; c) A. Laiho, B. M. Smarsly, C. F. J. Faul, O. Ikkala, *Adv. Funct. Mater.* **2008**, *18*, 1890–1897.
- [24] D. Franke, M. Vos, M. Antonietti, N. Sommerdijk, C. F. J. Faul, *Chem. Mater.* **2006**, *18*, 1839–1847.
- [25] Y. W. Huang, Y. Yan, B. M. Smarsly, Z. X. Wei, C. F. J. Faul, *J. Mater. Chem.* **2009**, *19*, 2356–2362.
- [26] a) Z. J. Chen, V. Stepanenko, V. Dehm, P. Prins, L. D. A. Siebbeles, J. Seibt, P. Marquetand, V. Engel, F. Würthner, *Chem. Eur. J.* **2007**, *13*, 436–449; b) S. Ghosh, X. Q. Li, V. Stepanenko, F. Würthner, *Chem. Eur. J.* **2008**, *14*, 11343–11357.
- [27] X. Yang, X. H. Xu, H. F. Ji, *J. Phys. Chem. B* **2008**, *112*, 7196–7202.
- [28] a) F. Würthner, Z. J. Chen, V. Dehm, V. Stepanenko, *Chem. Commun.* **2006**, 1188–1190; b) F. Würthner, C. Thalacker, S. Diele, C. Tschierske, *Chem. Eur. J.* **2001**, *7*, 2245–2253.
- [29] a) A. D. Q. Li, W. Wang, L. Q. Wang, *Chem. Eur. J.* **2003**, *9*, 4594–4601; b) W. Wang, J. J. Han, L. Q. Wang, L. S. Li, W. J. Shaw, A. D. Q. Li, *Nano Lett.* **2003**, *3*, 455–458; c) T. Heek, F. Würthner, R. Haag, *Chem. Eur. J.* **2013**, *19*, 10911–10921.
- [30] S. Yagai, T. Seki, T. Karatsu, A. Kitamura, F. Würthner, *Angew. Chem. Int. Ed.* **2008**, *47*, 3367–3371; *Angew. Chem.* **2008**, *120*, 3415–3419.
- [31] Z. Chen, B. Fimmel, F. Würthner, *Org. Biomol. Chem.* **2012**, *10*, 5845–5855.
- [32] a) J. van Herrikhuyzen, A. Syamakumari, A. Schenning, E. W. Meijer, *J. Am. Chem. Soc.* **2004**, *126*, 10021–10027; b) F. Würthner, Z. J. Chen, F. J. M. Hoeben, P. Osswald, C. C. You, P. Jonkheijm, J. von Herrikhuyzen, A. Schenning, P. van der Schoot, E. W. Meijer, E. H. A. Beckers, S. C. J. Meskers, R. A. J. Janssen, *J. Am. Chem. Soc.* **2004**, *126*, 10611–10618.
- [33] a) S. Bai, S. Debnath, N. Javid, P. W. J. M. Frederix, S. Fleming, C. Pappas, R. V. Ulijn, *Langmuir* **2014**, *30*, 7576–7584; b) C. Huang, S. Barlow, S. R. Marder, *J. Org. Chem.* **2011**, *76*, 2386–2407; c) S. Rehm, V. Stepanenko, X. Zhang, T. H. Rehm, F. Würthner, *Chem. Eur. J.* **2010**, *16*, 3372–3382.
- [34] a) M. Sauer, J. Hofkens, J. Enderlein in *Handbook of Fluorescence Spectroscopy and Imaging*, Wiley-VCH, Weinheim, **2011**, p. 282; b) F. Fennel, S. Wolter, Z. Xie, P.-A. Ploetz, O. Kuehn, F. Würthner, S. Lochbrunner, *J. Am. Chem. Soc.* **2013**, *135*, 18722–18725.
- [35] J. M. Lim, P. Kim, M.-C. Yoon, J. Sung, V. Dehm, Z. Chen, F. Würthner, D. Kim, *Chem. Sci.* **2013**, *4*, 388–397.
- [36] a) J. Kumar, T. Nakashima, H. Tsumatori, T. Kawai, *J. Phys. Chem. Lett.* **2014**, *5*, 316–321; b) J. Kumar, T. Nakashima, T. Kawai, *Langmuir* **2014**, *30*, 6030–6037.
- [37] F. Würthner, C. Thalacker, A. Sautter, W. Scharl, W. Ibach, O. Hollricher, *Chem. Eur. J.* **2000**, *6*, 3871–3886.
- [38] Z. J. Chen, U. Baumeister, C. Tschierske, F. Würthner, *Chem. Eur. J.* **2007**, *13*, 450–465.
- [39] The self-assembly behaviour of PDIs has also been described previously using a dimer model. An attempt was not made here to model the self-assembly of BTPPP using the dimer model, as it is very difficult to distinguish between the dimer and isodesmic models using only optical data.
- [40] R. B. Martin, *Chem. Rev.* **1996**, *96*, 3043–3064.
- [41] M. M. J. Smulders, M. M. L. Nieuwenhuizen, T. F. A. de Greef, P. van der Schoot, A. Schenning, E. W. Meijer, *Chem. Eur. J.* **2010**, *16*, 362–367.
- [42] a) F. Würthner, *Pure Appl. Chem.* **2006**, *78*, 2341–2349; b) B.-P. Jiang, D.-S. Guo, Y. Liu, *J. Org. Chem.* **2011**, *76*, 6101–6107.
- [43] A. Ustinov, H. Weissman, E. Shirman, I. Pinkas, X. Zuo, B. Rybtchinski, *J. Am. Chem. Soc.* **2011**, *133*, 16201–16211.
- [44] G. A. Bhavsar, S. K. Asha, *Chem. Eur. J.* **2011**, *17*, 12646–12658.
- [45] L. Xue, Y. F. Wang, Y. L. Chen, X. Y. Li, *J. Colloid Interface Sci.* **2010**, *350*, 523–529.

- [46] B. Gao, D. Xia, L. Zhang, Q. Bai, L. Bai, T. Yang, X. Ba, *J. Mater. Chem.* **2011**, *21*, 15975–15980.
- [47] Y. Huang, J. Hu, Z. Wei, C. F. J. Faul, *Chem. Commun.* **2011**, *47*, 5554–5556.
- [48] Y. Tidhar, H. Weissman, S. G. Wolf, A. Gulino, B. Rybtchinski, *Chem. Eur. J.* **2011**, *17*, 6068–6075.
- [49] V. Stepanenko, X.-Q. Li, J. Gershberg, F. Würthner, *Chem. Eur. J.* **2013**, *19*, 4176–4183.
- [50] D. Ke, A. Tang, C. Zhan, J. Yao, *Chem. Commun.* **2013**, *49*, 4914–4916.
- [51] K.-R. Wang, H.-W. An, Y.-Q. Wang, J.-C. Zhang, X.-L. Li, *Org. Biomol. Chem.* **2013**, *11*, 1007–1012.
- [52] F. J. M. Hoeben, P. Jonkheijm, E. W. Meijer, A. Schenning, *Chem. Rev.* **2005**, *105*, 1491–1546.
- [53] G. Klebe, F. Graser, E. Hadicke, J. Berndt, *Acta Crystallogr. Sect. B* **1989**, *45*, 69–77.
- [54] S. Singh, D. A. Dunmur, *Liquid Crystals: Fundamentals*, World Scientific, Singapore, **2002**.

---

Received: November 14, 2014

Published online on February 16, 2015